

Nanoscale

Accepted Manuscript



This is an *Accepted Manuscript*, which has been through the Royal Society of Chemistry peer review process and has been accepted for publication.

Accepted Manuscripts are published online shortly after acceptance, before technical editing, formatting and proof reading. Using this free service, authors can make their results available to the community, in citable form, before we publish the edited article. We will replace this *Accepted Manuscript* with the edited and formatted *Advance Article* as soon as it is available.

You can find more information about *Accepted Manuscripts* in the [Information for Authors](#).

Please note that technical editing may introduce minor changes to the text and/or graphics, which may alter content. The journal's standard [Terms & Conditions](#) and the [Ethical guidelines](#) still apply. In no event shall the Royal Society of Chemistry be held responsible for any errors or omissions in this *Accepted Manuscript* or any consequences arising from the use of any information it contains.

Nanotube Li_2MoO_4 : A Novel and High-Capacity Material as Lithium-Ion Batteries Anode

Xudong Liu¹, Yingchun Lyu³, Zhihua Zhang², Hong Li³, Yong-sheng Hu³, ZhaoXiang

Wang³, Yanming Zhao^{*1}, Quan Kuang¹, Youzhong Dong¹, Zhiyong Liang¹, Qinghua Fan¹, and

Liquan Chen³

1. State Key Laboratory of Luminescent Materials and Devices, South China University of Technology,

Guangzhou, 510640, P. R. China

2. Liaoning Key Materials Laboratory for Railway, School of Materials Science and Engineering,

Dalian Jiaotong University, Dalian 116028, China

3. Institute of Physics, Chinese Academy of Sciences, Beijing 100190, P. R. China

ABSTRACT: Carbon-coated Li_2MoO_4 hexagonal hollow nanotubes were fabricated via a facile sol-gel method involving the solution synthesis of Li_2MoO_4 with the subsequent annealing under an inert atmosphere to decompose the organic carbon source. To the best of our knowledge, this is the first report on the synthesis of Li_2MoO_4 nanotubes, more significantly, we, for the first time find Li_2MoO_4 can be as an anode material for lithium-ion batteries (LIBs). When evaluated as an anode material, the carbon-coated Li_2MoO_4 hollow nanotubes show an excellent electrochemical performance with a high reversible capacity ($\sim 550 \text{ mAh g}^{-1}$) after 23 cycles, good rate capability and cycling stability. Meanwhile, carbon-free Li_2MoO_4 sample fabricated via a solid state reaction was also prepared for comparison. The Li storage mechanism has been investigated by advanced XPS, in-situ XRD and HRTEM in detail below.

Keyword: Lithium-ion batteries, Anode, Carbon-coating, Sol-gel method, Nanotubes, Storage mechanism

INTRODUCTION

Lithium-ion batteries (LIBs) have been intensively utilized in portable electronics and show significant promise for the applications in hybrid electric vehicles (HEVs), electric vehicles (EVs), and smart grids. Graphite is used as the dominant anode in commercial LIBs, but its specific capacity is limited to 1 mol Li per C₆ (372 mAhg⁻¹). Besides, the Li intercalation into graphite appears at a low potential which is close to that of the Li-plating, which easily gives rise to the short circuit of batteries due to the formation of Li dendrites.^[1] All these issues related to graphite limit its application in the future, so, further improvements in terms of energy power, densities, cycle time and safety are required. Transition metal oxides have long been known as competitive anode materials for lithium-ion batteries due to their high reversible capacities and a higher potential relative to Li⁺/Li than graphite.^[2-9] Specially, molybdenum oxide MoO₃^[10-12] and a series of molybdate such as MMoO₄(M = Mn, Cu, Zn, Ni, Fe, Ca)^[13-15] have been reported about their electrochemical intercalation of lithium as possible anode materials for Li-ion batteries. Since Mo can exist in various oxidation states ranging from +6 to 0 during the conversion reaction process, they display large capacity at the beginning of the electrochemical process. However, the large capacity could not be sustained on long-term cycling for their conventional bulk electrode and poor electronic conductivity. It has been widely acknowledged that nanosized materials provide higher electrochemical performance both in cathode or anode by

means of decreasing lithium-ion diffusion distances and increasing the contact area between the electrode and the electrolyte.^[2,7,10-12] Therefore, nanosized the Mo-based compounds with special morphology is an effective way to fully release their higher capacities and keep an excellent electrochemical performance. Meanwhile, coating on the material surface is also a way to improve the electrochemical performance.^[13] Especially to improve the electronic conductivity, carbon coating on the surface of materials has been a general method, therefore, combination of these two measurements will be good for Mo-based electrode materials.

Inspired by this concept, in this contribution, we for the first time, give the experimental evidence on electrochemical performance of a lithium molybdenum oxide, Li_2MoO_4 , a high valence (+6) for the molybdenum, which could serve as a novel anode for Li-ion batteries, and for the first time, synthesize carbon-coated Li_2MoO_4 with a hexagonal hollow nanotube structure (short for nanotubes) on a large-scale via a simple sol-gel method. For comparison, the results for carbon-free Li_2MoO_4 powders (short for powders) prepared via a solid state reaction are also shown. The insertion/extraction behaviours of this novel anode material are demonstrated, which has a high specific capacity and excellent electrochemical performance in cycling stability and rate capability. These favourable properties suggest that Li_2MoO_4 is a novel and promising anode for advanced LIBs.

EXPERIMENTAL SECTION

Carbon-free powders Li_2MoO_4 was prepared via solid state reaction. Appropriate ratios of dried Li_2CO_3 (0.7540g) and MoO_3 (1.4467g) powders (Li: Mo = 2:1 in mol)

were mixed thoroughly using an agate mortar, then the mixture were annealed at 550°C for 12h in air using an temperature-controlled furnaces. Carbon-coated hollow nanotube Li_2MoO_4 was prepared via a sol-gel method. Li_2CO_3 (0.7540g), MoO_3 (1.4467g) powders (Li: Mo = 2:1 in mol) and citric acid ($\text{C}_6\text{H}_8\text{O}_7 \cdot \text{H}_2\text{O}$) 0.3520g as carbon source were dissolved in 100mL of distilled water under vigorous stirring to form a solution. Then, the mixed solution was heated to 80°C and maintained until the solution drying out. The obtained white gel was annealed at 400°C for 6h in ultrapure Ar atmosphere, followed by cooling to the room temperature.

Powder X-ray diffraction (XRD) patterns were collected with a Bruker D8 Advance Diffractometer using Cu $\text{K}\alpha$ radiation source ($\lambda_1 = 1.54060 \text{ \AA}$, $\lambda_2 = 1.54439 \text{ \AA}$) and a LynxEye_XE detector. The morphologies of the samples were examined by field-emission scanning electron microscopy (FE-SEM, Hitachi S-4800) Transmission electron microscope (TEM) images were taken using a JEOL 2010 microscope operated at 200 kV. XPS spectra were determined on an ESCALAB210 electron using Al $\text{K}\alpha$ radiation. The carbon content was verified by Vario EL (Elementar, Germany) CHNS Elemental Analyzer. Thermogravimetry analysis (TGA) curves were collected by a STA-449-F3 Thermal Analyzer (NETZSCH, the Germany) with a heating rate of 10 °C /min under air atmosphere flow.

The electrochemical performances of carbon-free Li_2MoO_4 powders and carbon-coated Li_2MoO_4 nanotube were measured with two-electrode electrochemical cells using a Land CT2001A battery tester (Land®, China). The anode film was prepared by mixing the as-synthesis sample with acetylene black and polyvinylidene

fluoride (PVDF) binder in a weight ratio of 8:1:1 in N-methyl-2-pyrrolidone (NMP). The obtained slurry was coated on Cu foil uniformly and the active material loading on electrode was 3mg. Two-electrode electrochemical cells were assembled in a Mikrouna glove box filled with ultra-high argon. Lithium metal foils were used as counter electrodes, Celgard 2320 as separator, and 1 M LiPF₆ in EC: DMC (1:1 vol. %) was used as electrolyte. Electrochemical impedance spectroscopy (EIS) was collected on an AUTOLAB PGSTAT302N (Metrohm, Netherlands). The impedance spectra were recorded by applying an *ac* voltage of 5mV in the frequency range from 1 MHz to 0.01 Hz. The in-situ XRD of nanotube were measured with two-electrode electrochemical cell where anode films were deposited on a Be window.

RESULT AND DISCUSSION

Here, we did a deep research including the morphology, structural changes, electrochemical performance and storage mechanism during the full electrochemical process.

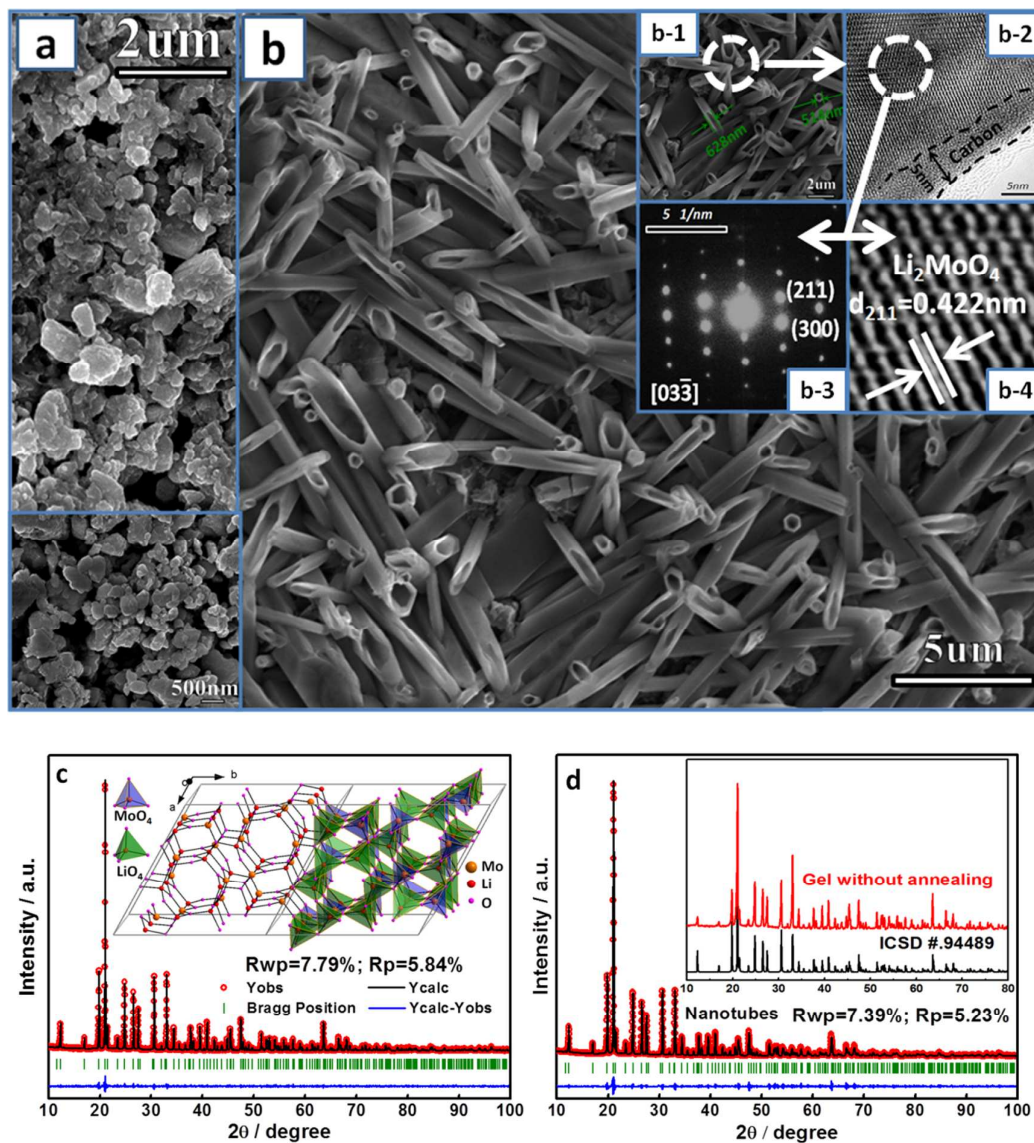


Figure 1. (a) SEM of powders and (b) SEM-TEM of nanotubes materials with indexed SAED pattern and HRTEM (b-2~b-4) obtained from large tubes. (c)&(d) XRD pattern and Rietveld analysis of the two samples; the inset in (c) shows the schematic structures of Li_2MoO_4 in which LiO_4 and MoO_4 tetrahedra are denoted by green and blue color, respectively.

The morphologies of Li_2MoO_4 prepared with different synthetic conditions are shown in **Figure 1a & b**, where the powders with the particle size less than $1 \mu\text{m}$ can be obtained (Figure 1a) via a solid state reaction method. As shown in Figure 1b, the nanotubes obtained via a sol-gel method are homogenous and have a hexagonal hollow structure with a characteristic diameter of less than $1 \mu\text{m}$ (Figure 1(b-1)). A

layer of amorphous carbon is coated on the nanotubes uniformly with a thickness of 5 nm (Figure 1(b-2)). It is believed that this can enhance the electronic conductivity of the Li_2MoO_4 effectively and improve the electrochemical performance. A typical lattice-resolved high-resolution transmission electron microscopy (HRTEM) image of nanotubes reveals that a single crystalline in nature with a d-spacing of 0.422 nm corresponds to the (211) crystal faces (Figure 1(b-4)). The corresponding selected area electron-diffraction (SAED) pattern taken along [03-3] crystal zone axis (Figure 1(b-3)) shows that the nanotubes adopt a single crystal structure which has a primitive trigonal structure and the lattice constant agrees well with our X-ray diffraction (XRD) measurement results. Figures 1c&d show the Rietveld refinement results of powders and nanotubes respectively, and a space group of $R\text{-}3H$ (ICSD card No.94489) was chosen as the structural refinement model. The reasonably small Rwp factor (7.79% & 7.39%) suggests that single-phase Li_2MoO_4 obtained under our experimental process has the unit cell parameters with $a=14.33013\text{\AA}$, $c=9.58331\text{\AA}$ and $a=14.32487\text{\AA}$, $c=9.57957\text{\AA}$ for powders and nanotubes from the results of the refinement. As shown in Figure 1d, no peaks related to impurities for nanotubes detected under the resolution of our X-ray diffractometer were observed, indicating that carbon-coating does not affect the trigonal structure of Li_2MoO_4 where the carbon content with 2.86% was verified in weight by the elemental analyzer. Li_2MoO_4 is isostructural with phenacite which consists of a three-dimensional network of corner-linked, slightly distorted LiO_4 and fairly regular MoO_4 tetrahedra (Figure 1c-inset) and these atomic arrangements present a narrow open channel along the

3-fold axis. The different morphologies might be caused by the different synthesis methods. In fact, the raw materials of MoO_3 and Li_2CO_3 react directly in water, which means, the Li_2MoO_4 phase can be obtained directly from the white gel after solution drying without further annealing (Figure 1d-inset). The role of annealing here is to make the organic carbon source decomposition and achieve the nanotubes products.

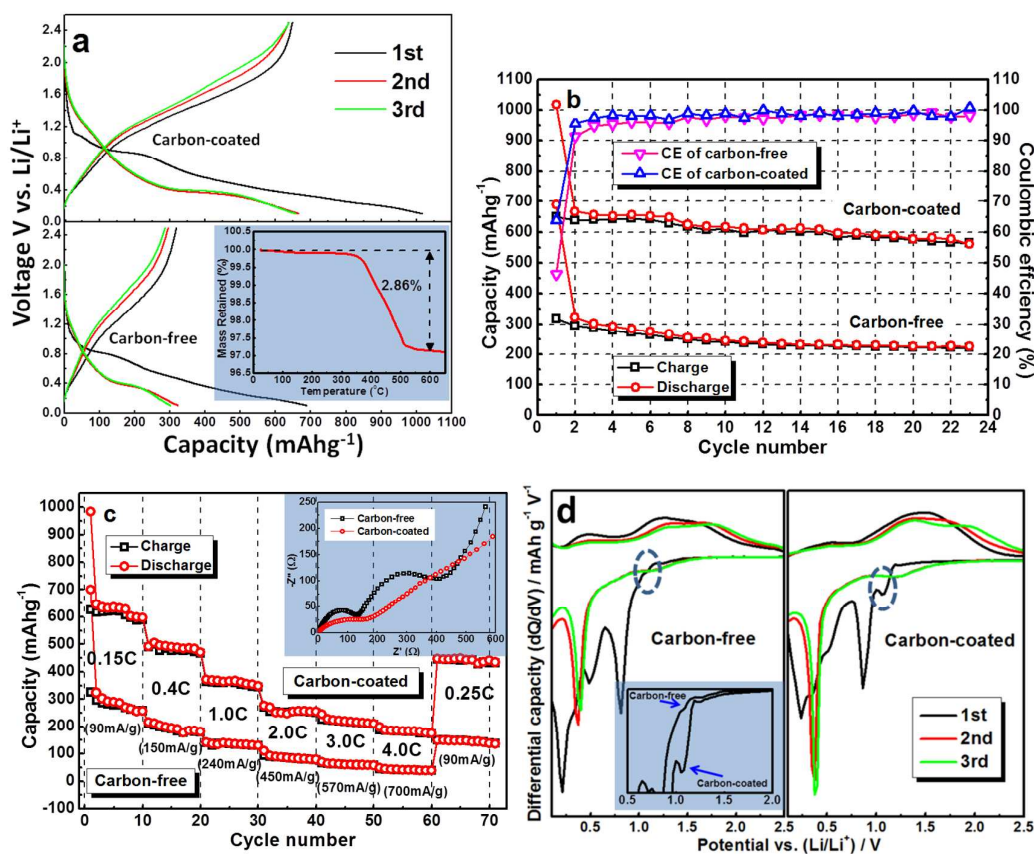


Figure 2. (a) The first three cycles of galvanostatic discharge/charge curves of powders and nanotubes, a TGA result as a inset. (b) Cycle performance and CE corresponding to Figure 2a at a current density of 90mA/g between 0.1~2.5V vs. Li/Li^+ . (c) Rate abilities of powders and nanotubes at various discharge/charge rates of 0.15C, 0.4C, 1.0C, 2.0C, 3.0C, 4.0C and finally 0.25C in succession, the EIS result as a inset. (d) The EVS differential capacity data corresponding to Figure 2a.

Figure 2a shows the typical charge-discharge curves for the first three cycles of the powder and nanotube electrodes. Considering a low potential, which results in a safety risk due to the formation of Li-plating, we choose 0.1V as the low cut-off

voltage. The first discharge and recharge capacities of nanotubes are $\sim 1000 \text{ mAh g}^{-1}$ and $\sim 650 \text{ mAh g}^{-1}$, while the corresponding powders' are $\sim 690 \text{ mAh g}^{-1}$ and $\sim 320 \text{ mAh g}^{-1}$. The initial coulombic efficiency (CE) of nanotubes is around 63.8% while the powders' is 46.3%, and both of them will quickly increase to 98% after several cycles and remain as nearly 100% thereafter (Figure 2b). The discharge capacity is larger than the recharge capacity, leading to the relatively poor initial CE. This is a common drawback for these high-capacity metal oxide anode materials caused by the great fading capacity between lithiation and delithiation, which can be attributed to the side reactions such as the formation of solid electrolyte interface (SEI) layer and the irreversible reaction during the first lithiation process which will be discussed in the following. The amorphous carbon content can be evaluated from TGA measurement as shown in Figure.2a-inset. The TGA was carried out from 25 to 650°C , with a heating rate of $10^\circ\text{C min}^{-1}$ in an air environment. The main weight loss about 2.86% from 300°C to 600°C is due to the oxidation of the amorphous carbon in air, which is in good agreement with the result by elemental analyzer. After the first cycle, the electrode reaction shows a high reversibility as the third cycle can repeat well both the curve shape and the specific capacity of the second cycle. From the second cycle, both of their discharge capacities slowly decrease along the cycle number, after 23 cycles, a charging capacity of $\sim 225 \text{ mAh g}^{-1}$ (powders) and $\sim 550 \text{ mAh g}^{-1}$ (nanotubes) was obtained, with capacity retention of 70% and 84% to the second cycle shown in Figure 2b.

Figure 2c shows the rate capability of powders and nanotubes at various

discharge/charge rates. In the 1st-10th cycle, they have reversible discharge-charge capacity of $\sim 280 \text{ mAh g}^{-1}$ and $\sim 600 \text{ mAh g}^{-1}$ at 90 mA g^{-1} which is consistent with the cycling stability in Figure 2b. However, the nanotube electrodes can still deliver a good fraction of its total capacity $\sim 200 \text{ mAh g}^{-1}$ when it operated at a current rate as high as 4 C, while only $\sim 40 \text{ mAh g}^{-1}$ for powder electrodes. As the current rate changed from 4 C to 0.25 C after 60 cycles, a considerable higher capacity ($\sim 450 \text{ mAh g}^{-1}$ vs. 372 mAh g^{-1} for graphite) can be recovered for the nanotubes electrodes compared to powder electrodes ($\sim 150 \text{ mAh g}^{-1}$), indicating a good rate as well as a good cycling capability of the nanotube electrodes. The reason behind the good cycling performance and rate capability of the sample can be ascribed to the smaller size of particles and the effective amorphous carbon coating on it. Furthermore, the coated carbon gave rise to improvement of conductivity. Figure.2c-inset shows the electrochemical impedance spectrum (EIS) of the powder and nanotube electrodes which were measured after running three charge-discharge circles. All profiles in the figure exhibit depressed semicircles in the high and intermediate frequency region and a line in the low frequency region. The high-frequency semicircle is assigned to the SEI film and/or contact resistance; the semicircle in medium-frequency region is assigned to the charge-transfer impedance on electrode/electrolyte interface, and the inclined line in the low frequency region corresponds to the lithium-diffusion process within electrodes. It is clear to observe that the radius of the semicircle, at the intermediate frequency region for the nanotube electrode is smaller than the powders'. This may indicate lower charge-transfer

impedances and could mean that the coated carbon had improved the electronic conductivity, which in turn contributed to the improved cycling properties.

Figure 2d shows the first three consecutive electrochemical voltages spectroscopy (EVS) differential capacity curves of the powders and nanotubes electrodes corresponding to Figure 2a. It is obviously that there is a small oxidation peak around 1.1V (vs. Li/Li⁺) during the first discharge for the nanotubes', in fact, there is also a smaller one for the carbon-free powders', although the peak intensity is much weaker than that of carbon-coated nanotubes' shown in Figure 2d as an inset. This small peak around 1.1 V could be attributed to the side reaction during the lithium intercalation process if considering the similarity of the EVS curves between powders' and nanotubes' in the following cycles. Considering the similarity of the EVS curves between powders' and nanotubes' in the following, here, we only conducted the X-ray photoelectron spectroscopy (XPS) on nanotube electrodes to illustrate the changes of binding energy of Mo3d, C1s and O1s at different lithiation and delithiation states during the first cycle shown in **Figure 3a&b**. At 1.2 V during lithiation no obvious peaks can be observed in EVS curves above this voltage (Figure 2d), and the binding energy can be indexed to the Li₂MoO₄ (232.2 eV) phase accurately (Figure 3(a-1)). Mo³⁺ (230.6 eV), Mo²⁺ (228.6 eV) and metallic Mo (226.7 eV) were detected on further lithiation to 0.38 V combining with the specific capacity (~600 mAh g⁻¹) (Figure 3(a-2)). When discharged to 0.1 V, only metallic Mo is detected on the surface of the electrode (Figure 3(a-3)), which agrees well with our in-situ XRD (Figure 4) and TEM-EDS analysis (Figure 5). After recharged to 2.5 V,

the binding energy of nanotubes is not recovered, but a mixture valence state of Mo⁴⁺ (229.5 eV) and Mo⁵⁺ (231 eV) (Figure 3(a-4)). From the fitting results, the areas obtained for the Mo, Mo²⁺, Mo³⁺, Mo⁴⁺ and Mo⁵⁺ peaks can be used to calculate the approximate concentration ratio between them, according to:

$$\frac{N_{\text{Mo}^{x+}}}{N_{\text{Mo}^{y+}}} = \frac{I_{\text{Mo}^{x+}}}{I_{\text{Mo}^{y+}}} \quad (1)$$

where $I_{\text{Mo}^{x+}}$ and $I_{\text{Mo}^{y+}}$ represent the integral areas under their curves of the Mo3d peaks. By this calculation based on Equation (1), the approximate concentration ratios of 2.28:1.04:1 for Mo³⁺, Mo²⁺ to Mo (0.38 V, average for Mo^{2.06+}) and 2.37:1 for Mo⁴⁺ to Mo⁵⁺ (2.5 V, average for Mo^{4.3+}) with the calculated specific capacity of 606 mAh g⁻¹ and 661 mAh g⁻¹ in the nanotube electrodes, which are close to the real capacity ~600 mAh g⁻¹ and ~650 mAh g⁻¹ obtained in Figure 2a. The peaks of Mo 3d (Figure 3a) becomes weaker during the lithiation and delithiation process could be attributed to the growth of SEI layer. In fact, the growth process of SEI layer can be confirmed by the changes of binding energy of C1s and O1s, suggesting the existence of Li₂CO₃ and ROCO₂Li as shown in Figure 3b. The overlapping of EVS curves after first cycle (Figure 2d) reveals the good reversibility of electrochemical reactions, and the difference of discharge EVS curves with that in subsequent cycling procedure (Figure 2d) might be due to the irreversible structure destruction, which is confirmed by the following in-situ XRD (Figure 4) and TEM (Figure 5) analysis.

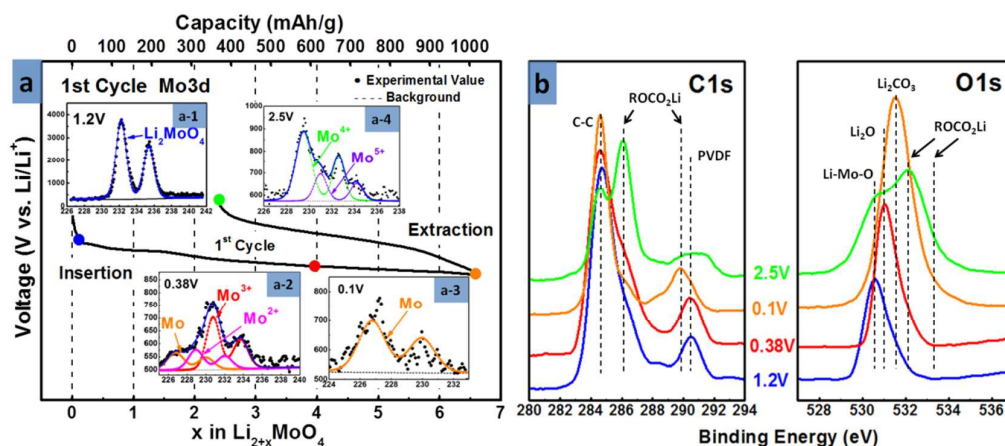
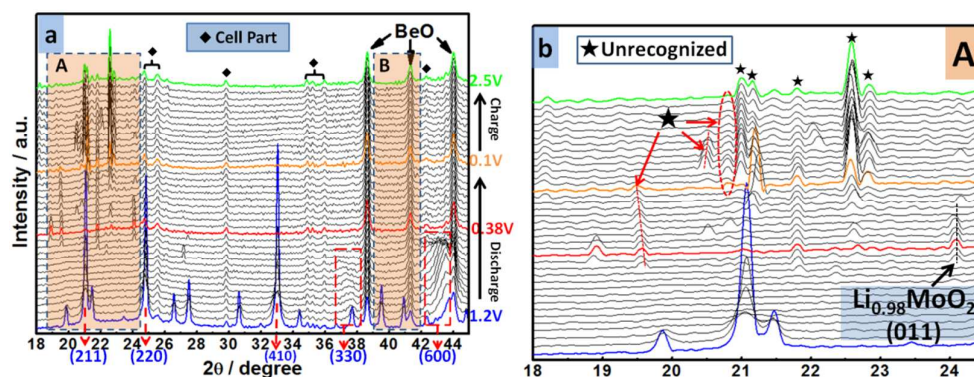


Figure 3. XPS of nanotube electrodes discharged to 1.2V, 0.38V, 0.1V and charged to 2.5V, (a) Mo3d and (b) C1s, O1s in the first cycle.

To investigate the structural changes upon Li insertion/extraction, we conducted the in-situ XRD measurements on the nanotube electrodes and selected two regions (A & B) to show the evolution of main peaks as shown in **Figure 4**. Firstly, Figure 4a shows some systematic peaks which appear throughout the experiment, that is, peaks marked "Cell Part"(denoted hereafter \blacklozenge) and "BeO".^[14] During the electrode discharged to 1.2 V (blue line), a well-defined Li_2MoO_4 phase can be confirmed. The vanished and broadening peaks accompanied by a slight shift on further lithiation with d-spacing of (211), (220), (410) and (330), (600) imply amorphization and lattice expansion during the first lithiation.



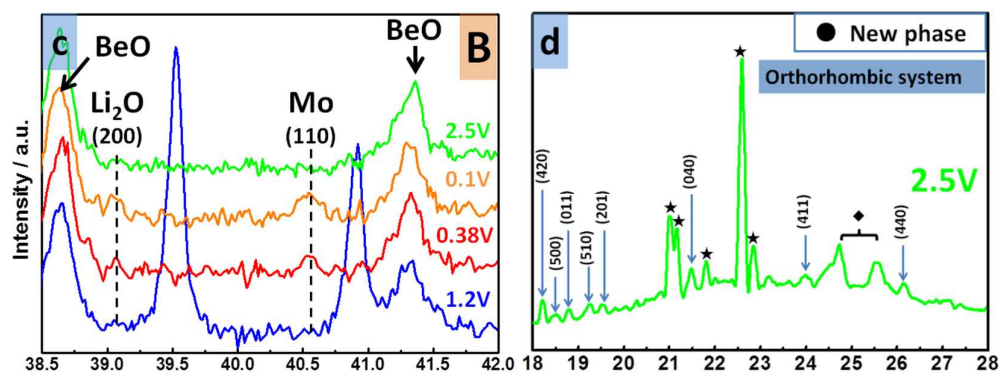
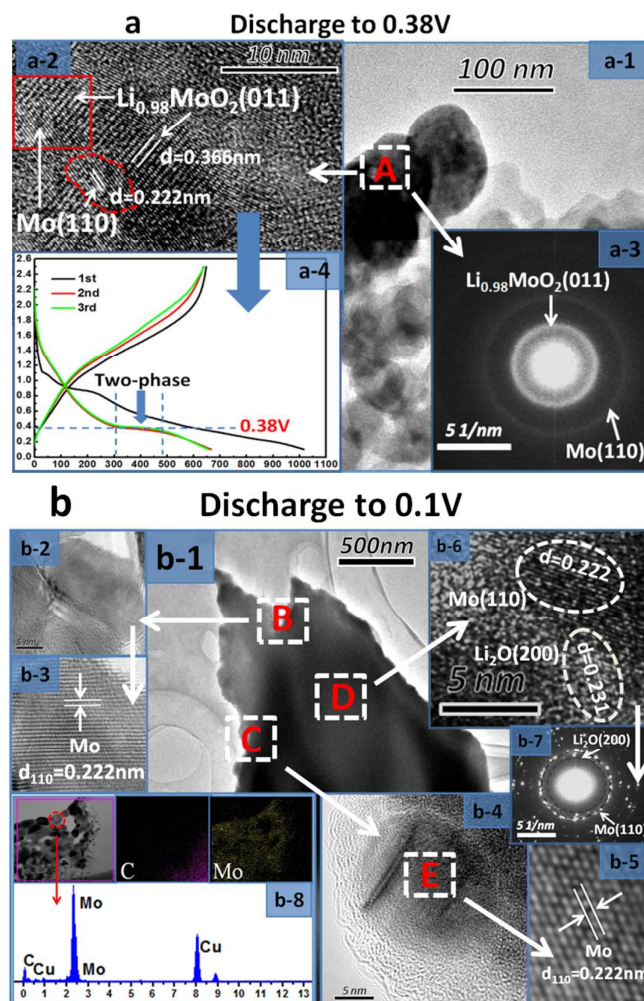


Figure 4. (a), (b) & (c) In-situ XRD patterns collected at various states of nanotube electrodes with a current density of 30 mA g^{-1} between 0.1~2.5 V vs. Li^+/Li for the first cycle (with an interval of 80 min taken one XRD pattern and 15 min for each 20 scan from 18° to 45°). (d) A calculation result for the final XRD at 2.5 V.

When discharged to 0.38 V, the peaks at 24.2° and 40.6° (red line) in regions A and B can be indexed to structure of $\text{Li}_{0.98}\text{MoO}_2$ (ICSD card No.201481) and metallic Mo (ICSD card No.173131) respectively, which is consistent with binding energies of Mo^{3+} and Mo in XPS (Figure 3(a-2)). It should be noted that it is difficult to attribute the peaks (denoted hereafter ★) to any molybdenum oxide or lithium molybdenum oxide compounds accurately but the intermediate and final products in region A. The peaks of metallic Mo and Li_2O (ICSD card No.54368) can be confirmed during further lithiation to 0.1 V (orange line) in region B, although, the diffraction intensity is weaker which indicates a structure containing nano-crystal Mo and Li_2O with highly disordered. When recharged to 2.5V, the crystal structure of Li_2MoO_4 is irreversible, but the XRD patterns (Figure 4d) were successfully indexed in an orthorhombic cell (O-phase) with lattice constants $a=23.96722 \text{ \AA}$, $b=16.51071 \text{ \AA}$, $c=4.91028 \text{ \AA}$ and $V =1943.08 \text{ \AA}^3$ using Dicvol program,^[15] specially, the lattice spacing of 0.485 nm and 0.413 nm in Z_1 and Z_2 (Figure 5(c-2)) regions agree well with the d-spacing of (420) and (040) crystal faces calculated from our in-situ XRD.

Considering the recharging specific capacity ($\sim 650 \text{ mAh g}^{-1}$) and in-situ XRD (Figure 4d), a structure of ‘ Li_xMoO_y ’ with $\text{Mo}^{4.3+}$ (average of Mo^{4+} and Mo^{5+}), which is corresponding to the calculation of XPS in Figure 3a, can be inferred to describe this delithiation product.^[16-23] It believes that this O-phase is responsible for electrochemical performance in the following cycles.

The corresponding ex-situ TEM-EDS results of the electrode as discharged to 0.38 V, 0.1 V, and then recharged to 2.5 V are shown in **Figure 5**.



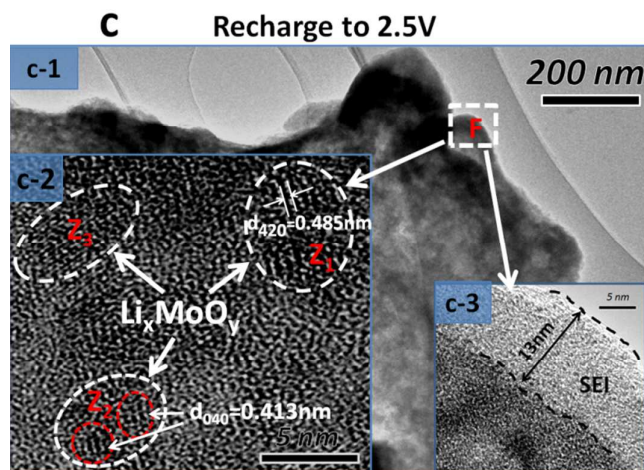


Figure 5. SEM, TEM-EDS analysis of nanotubes discharged to 0.38V (a), 0.1V (b), and then recharged to 2.5V (c) with a current density of 30mA g^{-1} between 0.1~2.5V vs. Li/Li^+ in the first cycle.

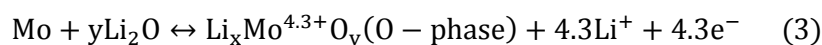
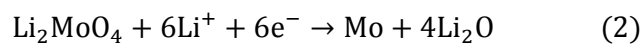
Two phases of $\text{Li}_{0.98}\text{MoO}_2$ and metallic Mo can also be confirmed by HRTEM (Figure 5(a-2)) and SAED (Figure 5(a-3)), where the transition region is not completely disordered, and probably supports a composition gradient that allows the two phases to coexist despite the lattice mismatch, which might be responsible for the two-phase reaction at about 0.38V (Figure 4(a-4)) in the following cycles.

After fully discharged to 0.1 V, three selected areas coming from the edge (B & C) and internal local area (D) of the larger cluster (Figure 5(b-1)) were focused for further HRTEM and SAED analysis. In Figure 5(b-2~5), well-defined stripes with a d-spacing consistent of (110) crystal face can be confirmed as nano-crystal metallic Mo. In the internal local area D (Figure 4(b-6&7)), reveals the existence of Mo and Li_2O which is consistent with the results of the in-situ XRD pattern (Figure 4b). The corresponding EDS and mapping imaging (Figure 5(b-8)) reveals the absence of oxygen in the area B, also, an existence evidence of metallic Mo particles after full discharged to 0.1 V. Combined with the high capacity ($\sim 1000\text{mAh g}^{-1}$) observed previously, we can infer that metallic Mo and Li_2O are two main final products in the

nanotube electrodes discharged to 0.1V for the first cycle relative to the theoretical capacity (924 mAh g⁻¹).

When recharged to 2.5V, although, the electrode materials have been amorphous seriously revealed by the HRTEM imaging (Figure 5c), some nano-crystal domains can still be recognized (Figure 5(c-2)). Specially, the lattice spacing of 0.485 nm and 0.413 nm in Z₁ and Z₂ regions agree well with the d-spacing of (420) and (040) crystal faces calculated from our in-situ XRD (Figure 4d). It indicates that although the structure is disordered, it has not become completely amorphous. The irreversible reduction of Li₂MoO₄ to metallic Mo and Li₂O is believed to be a main reason for the large capacity fading besides the formation of SEI layer, although the SEI layer has a thickness of about 13 nm after delithiation (Figure 5(c-3)). However, in contrast with the as-prepared well-defined tubular structure, the nanotubes have been destroyed completely up to 0.38 V, 0.1 V and highly powdered when recharged to 2.5 V respectively.

Based on the above structural analysis and a mechanism for Li insertion in Na_{0.25}MoO₃ and CaMoO₄,^[19-21,24] the nanotube structure of Li₂MoO₄ is irreversible upon Li⁺ insertion/extraction, however, the relative good cycle performance except the first cycle suggest that a reversible electrochemical process exist after the first delithiation shown in Fig.2b & 2c. So, the following conversion reaction mechanism is proposed for Li₂MoO₄ system:



Where $2y=x+4.3$. According to the amount of Li^+ /mol insertion observed, a total of 6.6mol Li^+ per formula are inserted in the initial discharge process (Figure 3a), 6mol Li^+ are for the conversion reaction (Equation (2)) corresponding to the theoretical capacity (924 mAh g^{-1}), and the extra 0.6 mol Li^+ could be attributed to the formation of SEI layer and the polymeric gel-type layer on the metal nanoparticles due to the decomposition of the solvent in the electrolyte. The electrode materials during recharged to 2.5V is a composite electrodes made up of an amorphous containing nanocrystalline $\text{Li}_x\text{Mo}^{4.3+}\text{O}_y$ (O-phase), and this O-phase of Li-Mo-O matrix is responsible for the subsequent discharge/charge cycles (Equation (3)).

CONCLUSION

Carbon-free sample and carbon-coated hexagonal hollow nanotube Li_2MoO_4 have been synthesized by a solid state reaction and sol-gel method on a large-scale respectively. Our experimental results showed that nanotube Li_2MoO_4 delivers a high reversible specific capacity ($\sim 550 \text{ mAh g}^{-1}$) compared to the powders' ($\sim 225 \text{ mAh g}^{-1}$) after 23 cycles and a significantly enhanced electrochemical performance in terms of cycling stability and rate capability. A reduction accompanied by metallic Mo contributes to the large the specific capacity ($\sim 1000 \text{ mAh g}^{-1}$) in the first lithiation process. Although the nanotube structure of Li_2MoO_4 is irreversible upon Li insertion/extraction during the first cycle, a structure of ' $\text{Li}_x\text{Mo}^{4.3+}\text{O}_y$ ' can be successfully indexed in an orthorhombic cell (O-phase). Meanwhile, the structure is disordered, but it has not become completely amorphous. However, further investigations about improvements including optimization and strengthening the

nanotube structure during the electrochemical process and accurately solving the O-phase structure of this material still need to be done in the future.

AUTHOR INFORMATION

* **Corresponding author.** Tel.: +86-20-87111963, Fax: +86-20-85511266

E-mail address: zhaoym@scut.edu.cn;

Notes: The authors declare no competing financial interest.

ACKNOWLEDGEMENTS

This work was funded by NSFC Grant (No.51172077) supported through NSFC Committee of China, and the Foundation of (No.S2011020000521) supported through the Science and Technology Bureau of Guangdong Government.

REFERENCES

- (1) S.S. Zhang, *J. Power Sources*. **2006**, *161*, 1385.
- (2) P. Poizot, S. Laruelle, S. Grugeon, L. Dupont, J.M. Tarascon, *Nature*. **2000**, *407*, 496.
- (3) S. Laruelle, S. Grugeon, P. Poizot, M. Dolle, L. Dupont, J.M. Tarascon, *J. Electrochem. Soc.* **2002**, *149*, A627.
- (4) W.Y. Li, L.N. Xu, J. Chen, *Adv. Funct. Mater.* **2005**, *15*, 851.
- (5) P.L. Taberna, S. Mitra, P. Poizot, P. Simon, J.-M. Tarascon, *Nature Mater.* **2006**, *7*, 567.

- (6) W.M. Zhang, X.L. Wu, J.S. Hu, Y.G. Guo, L.J. Wan, *Adv. Funct. Mater.* **2008**, *18*, 3941.
- (7) P.G. Bruce, B. Scrosati, J.-M. Tarascon, *Angew. Chem. Int. Ed.* **2008**, *47*, 2930.
- (8) M. S. Whittingham, *Chem. Rev.* **2004**, *104*, 4271.
- (9) M. S. Whittingham, *Science.* **1976**, *192*, 1126.
- (10) C. H. Jiang, E. Hosono, H. S. Zhou, *Nano.Today.* **2006**, *1*, 28.
- (11) Z. Y. Wang, L. Zhou, X. W. Lou, *Adv. Mater.* **2012**, *24*, 1903.
- (12) Chao Luo, Ruiming Huang, Ruslan Kevorkyants, Michele Pavanello, Huixin He, Chunsheng Wang, *Nano Letters.* **2014**, *14*, 1596.
- (13) Chao Luo, Yujie Zhu, Yang Wen, Jingjing Wang, Chunsheng Wang, *Adv. Funct. Mater.* **2014**, *24*, 4082.
- (14) Ian A. Courtney, J. R. Dahn, *J. Electrochem. Soc.* **1997**, *144*, 2045.
- (15) Boultif, A. Louer, D. *J. Appl. Crystallogr.* **2004**, *37*, 724.
- (16) Hara, D. Shirakawa, J. Ikuta, H. Uchimoto, Y. Wakihara, M. Miyanaga, T. Watanabe, I. *J. Mater. Chem.* **2002**, *12*, 3717.
- (17) Hara, D. Ikuta, H. Uchimoto, Y. Wakihara, M. *J. Mater. Chem.* **2002**, *12*, 2507.
- (18) Hara, D. Shirakawa, J. Ikuta, H. Uchimoto, Y. Wakihara, M. Miyanaga, T. Watanabe, I. *J. Mater. Chem.* **2003**, *13*, 897.
- (19) Nazar, L. F. Goward, G. Leroux, F. Duncan, M. Huang, H. Kerr, T. Gaubicher, J. *Intl. J. Inorg. Mater.* **2001**, *3*, 191.
- (20) Leroux, F. Nazar, L. F. *Solid State Ionics.* **2000**, *133*, 37.

- (21) Leroux, F. Goward, G. R. Power, W. P. Nazar, L. F. *Electro-chem. Solid-State Lett.* **1998**, *1*, 255.
- (22) Kim, S. S. Ogura, S. Ikuta, H. Uchimoto, Y. Wakihara, M. *Chem. Lett.*(Japan) **2001**, 760.
- (23) Kim, S. S. Ogura, S. Ikuta, H. Uchimoto, Y. Wakihara, M. *Solid State Ionics.* **2002**, *146*, 249.
- (24) N. Sharma, K.M. Shaju, G.V. Subba Rao, B.V.R. Chowdari, Z.L.Dong, T.J. White, *Chem. Mater.* **2004**, *16*, 504.